https://doi.org/10.5194/tc-2023-77
Preprint. Discussion started: 9 June 2023

The Cryosphere Discussions

Coupled ice/ocean interactions during the future retreat of West Antarctic ice streams

David T. Bett[1], Alexander T. Bradley[1,2], C. Rosie Williams[1], Paul R. Holland[1], Robert J. Arthern[1] and Daniel N. Goldberg[3]

[1]British Antarctic Survey, Cambridge, UK
[2]Cambridge Zero, Cambridge, UK
[3]University of Edinburgh, Edinburgh, UK

Correspondence to: David T. Bett (d.bett@bas.ac.uk)

Abstract.

The Amundsen Sea sector has some of the fastest-thinning ice shelves in Antarctica, caused by high, ocean-driven basal melt rates, which can lead to increased ice stream flow, causing increased sea level rise (SLR) contributions. In this study, we present the results of a new synchronously coupled ice-sheet/ocean model of the Amundsen Sea sector. We use the WAVI ice sheet model to solve for ice velocities and the MITgcm to solve for ice thickness and three-dimensional ocean properties, allowing for full mass conservation in the coupled ice/ocean system. The coupled model is initialised in the present day and run forward under idealised warm and cold ocean conditions. We find that Thwaites Glacier dominates the future SLR from the Amundsen Sea sector, with a SLR that is approximately quadratic in time. The future evolution of Thwaites Glacier depends on the life-span of small pinning points that form during the retreat. The rate of melting around these pinning points provides the link between future ocean conditions and the SLR from this sector and will be difficult to capture without a coupled ice/ocean model. Grounding-line retreat leads to a progressively larger Thwaites ice-shelf cavity, leading to a positive trend in total melting, resulting from the increased ice basal surface area. Despite these important sensitivities, Thwaites Glacier retreats even in a scenario with zero ocean-driven melting. This demonstrates that a tipping point may have been passed and some SLR from this sector is now committed.

1 Introduction

The West Antarctic Ice Sheet (WAIS) is a marine ice sheet of particular importance for future sea level rise (SLR), contributing ~6.5 mm to global SLR between 1992 to 2021 (Otosaka et al., 2023). Within the WAIS, the Amundsen Sea sector has seen the largest SLR contribution over the satellite era (Shepherd et al., 2019). The region experienced a 77% ice mass flux increase from 1973 to 2013, with the Thwaites Ice Shelf specifically observing a 33% speedup during this period (Mouginot et al., 2014).

https://doi.org/10.5194/tc-2023-77
Preprint. Discussion started: 9 June 2023

The Amundsen Sea sector's ice sheet is grounded on bathymetry below sea level, and the presence of retrograde slopes in the bathymetry may make the region susceptible to rapid and sustained retreat in the future (Favier et al., 2014). Any reduction in ice shelf buttressing via pinning points and side drag can lead to acceleration in ice shelf speed and retreat of the grounding line (Thomas, 1979). Ocean melting can reduce buttressing by thinning ice shelves, reducing side drag and aiding the ungrounding of pinning points. Of particular concern is Thwaites Glacier, whose current pinning point on its eastern ice shelf appears to be weakening, and has been predicted to unground within decades (Wild et al., 2022).

In the Amundsen Sea, warm modified Circumpolar Deep Water (CDW) resides below a colder and fresher layer of Winter Water (Jacobs et al., 1996), and flows through bathymetric troughs to the base of ice shelves (Walker et al., 2007), causing high melt rates. The region experiences large decadal variability in its ocean conditions, most notably in the thickness of the modified CDW layer (Jenkins et al., 2018; Dutrieux et al., 2014). In addition, it has been suggested that there is an average anthropogenic warming trend superimposed on this internal variability (Holland et al., 2022; Naughten et al., 2022). Future anthropogenic warming of the Amundsen Sea is a key mechanism by which human activities may influence SLR from the Antarctic Ice Sheet (Holland et al., 2022; Jourdain et al., 2022; Holland et al., 2019).

Previous studies have used uncoupled ice-only simulations to simulate the future evolution and retreat of the Amundsen Sea sector and WAIS (e.g. Yu et al., 2018; Alevropoulos-Borrill et al., 2020; Feldmann and Levermann, 2015; Reese et al., 2020). However, these studies use simple ocean melting parametrisations and hence lack spatial variation in melt rates caused by differences in ocean velocity and temperature. Therefore, these models incompletely represent the complex interactions between ice shelf geometry, ocean dynamics and melt rates, potentially leading to overestimations in rates of grounding line retreat and mass loss (Seroussi et al., 2017; De rydt and Gudmundsson, 2016). To accurately simulate ice evolution, a coupled ice/ocean model must be used.

Previous coupled modelling studies have used different approaches to the coupling using either an 'asynchronous' (e.g. Seroussi et al., 2017; De rydt and Gudmundsson, 2016; Naughten et al., 2021) or a 'synchronous' coupling (e.g. Goldberg and Holland, 2022; Goldberg et al., 2018; Jordan et al., 2018). Synchronous coupling involves continuously changing the ice geometry during the ocean simulation at the ocean model timestep, while asynchronous coupling involves information being exchanged every one or few ice model timesteps, with the ice geometry and ocean state modified at each coupling period. Regional coupled models have been used to simulate parts of the Amundsen Sea sector, for example simulating Thwaites Glacier over 50 years (Seroussi et al., 2017), and the Pope, Smith and Kohler glaciers (Goldberg and Holland, 2022).

In this study we use a new synchronously coupled ice/ocean model of the Amundsen Sea sector to simulate the evolution of its ice streams over the next 125 years. We consider three different idealised forcing scenarios: no basal melting, and cold and warm Amundsen Sea conditions. We use these simulations to explore both the future evolution of the ice sheet in this sector,

https://doi.org/10.5194/tc-2023-77
Preprint. Discussion started: 9 June 2023

and the physical processes that determine the speed of the retreat. This allows us to better understand the mechanisms by which the ice loss is sensitive to future ocean conditions, and thus to anthropogenic forcing.

2 Methods

2.1 Ice model

In the coupled ice/ocean model, ice velocities are calculated using the Wavelet-based, Adaptive-grid, Vertically Integrated ice sheet model, WAVI (Arthern et al., 2015; Arthern and Williams, 2017). We use a numerical model with a 2 km horizontal resolution covering the whole Amundsen Sea sector domain shown in Figure 1a, with a time step of 20 days. A Weertman' sliding law is used (Weertman, 1964), for which basal drag scales with the cube root of sliding velocity, multiplied by a drag coefficient C. As described in Arthern et al. (2015), WAVI uses a data assimilation method to match modelled ice velocities and rates of thickness changes with observations (Smith et al., 2020; Mouginot et al., 2017b; Mouginot et al., 2017a), resulting in an initial state representing conditions in approximately 2015. An ice model relaxation is then run for a set period of time (4000 years) in order to bring the flux divergence into better agreement with observations of accumulation and rates of ice thickness change (see Arthern et al. 2015 for full details). Ice thickness prior to relaxation and bathymetry fields are from BedmachineV3 (Morlighem et al., 2020; Morlighem, 2022). The ice front and outer catchment boundaries are kept fixed throughout the simulations. Accumulation and englacial temperatures are kept constant in the forward simulations (Arthern et al., 2006; Pattyn, 2010).

2.2 Ocean model

We use the Massachusetts Institute of Technology general circulation model (MITgcm; (Marshall et al., 1997)) to simulate the ocean circulation in the Amundsen Sea. The model grid uses polar stereographic Cartesian coordinates with horizontal resolution of 2 km and vertical resolution of 20 m, and we use a time step of 200 seconds. The ocean model domain extent is shown by the black box in Figure 1a. Note that this does not include the whole continental shelf, so we apply ocean boundary conditions and velocities to the northern and western open boundaries of the domain to impose prescribed Amundsen Sea conditions in idealised 'warm' and 'cold' experiments. We also examine a third 'no melting' case in which no ocean-driven melting is applied to the ice shelves. This study focuses solely on the ice sheet, ice shelf and ocean interactions driven by wider Amundsen Sea conditions, so sea ice and other freshwater sources/sinks are not included in the simulations, and no atmospheric forcing is applied over the model domain.

The boundary conditions in warm and cold experiments are as follows. Following previous studies, an idealised, piecewise linear, vertical profile is applied to replicate the warm CDW layer below cold Winter Water, with a thermocline 400 m thick (De Rydt et al., 2014). The base of the thermocline is placed at 600 m depth in the warm scenario and lowered to 800 m depth in the cold scenario (Figure 1c, d). These profiles correspond to the warmest and coldest observed Amundsen Sea conditions,

https://doi.org/10.5194/tc-2023-77
Preprint. Discussion started: 9 June 2023

respectively (Dutrieux et al., 2014). On the northern boundary the warm CDW layer has temperature of 1.2°C and a salinity of 34.7 (PSU), whereas the eastern boundary is forced with a more modified CDW layer, with temperature 0.6°C and salinity 34.6 (PSU) (Figure 1c, d). In all simulations, at the boundaries, we apply average ocean velocities (1965-2015) from a larger regional model (Holland et al., 2022; Naughten et al., 2022), and we restore sea level to zero.

Ocean only simulations, with fixed initial ice geometry, are simulated for 2 years, as a spin up before coupling. The resultant conditions in the ocean model are designed to match the spatial distribution of present day observed maximum subsurface temperatures over the region (Dutrieux et al., 2014), as shown in Figure 2a,b. The warm and cold oceanic forcing cases enable different amounts of CDW to reach the base of the present day Thwaites and Pine Island Glacier (PIG) ice shelves (Figure 2e, f, i, j). The initial melt rates of the Thwaites and PIG ice shelves for the warm and cold simulations are shown in Figure 2c, d, g, h.

Ice shelf melting is represented by a standard three-equation formulation (Holland and Jenkins, 1999). We tune the drag coefficient in this parametrization to 0.01 (Jenkins et al., 2010). For PIG and Thwaites ice shelves combined, this value produces the closest average match of the MITgcm ice shelf melt rates and those that are implicit in the WAVI initialisation (see Appendix A). This minimises the 'coupling shock' that occurs when the coupled model simulation commences. Without this calibration, the ice sheet trajectory could be impacted by the adjustment of the ice due to the step from implicit initialised melt rates to arbitrarily different ocean model melt rates at the start of the simulation. Note also that this tuned value agrees with a value derived from observations (Jenkins et al., 2010).

2.3 Ice/Ocean coupling

This study uses a new, synchronously coupled ice/ocean model, which combines the WAVI ice sheet model with the MITgcm. Crucially, this coupling occurs through the MITgcm ice sheet package STREAMICE (Goldberg and Heimbach, 2013), making use of previous synchronous coupling developments (Jordan et al., 2018; Goldberg et al., 2018). The basic concept of the new model is that WAVI solves for the ice velocities, MITgcm STREAMICE solves for the ice thickness, and the MITgcm ocean model solves for all ocean properties, including melting. Dividing up computations in this way allows for a fully synchronous coupling because both the ice thickness and ocean properties are solved within the MITgcm on the ocean timestep. This has two advantages: firstly, the ice thickness and ocean free surface equations are solved simultaneously, allowing full conservation of mass in the ice and ocean coupled system. Secondly, the melt rate responds instantly to changes in ice thickness.

In principle, this approach is no more expensive than other coupling approaches because the two-dimensional ice thickness equations can be solved on the ocean timestep with negligible computational expense compared to that incurred in solving three-dimensional ocean equations. However, the approach does require the MITgcm ocean grid to exist wherever ice may go afloat during the simulation, since grounding-line retreat is accomplished naturally, by inflating the water column in the

https://doi.org/10.5194/tc-2023-77
Preprint. Discussion started: 9 June 2023

MITgcm ocean model wherever the pressure loading of the ice decreases below floatation (Goldberg et al., 2018). In regions of ice which are not floating, a thin subglacial layer exists, which we set to be 4 m thick. This layer, which has no effect on basal drag computed by the ice model, is treated as a porous medium, with Darcy flow used to connect the subglacial cells to each other (Goldberg et al., 2018).

Using an MITgcm domain covering the entire catchment of Amundsen Sea sector would be very inefficient, since it would include large areas of grounded ice that in the 3D ocean grid that would never go afloat. To avoid this, we introduce the concept of 'ice-only' and 'coupled' domains (Figure 1a): In the ice-only domain, WAVI is used to solve for both ice sheet velocities and thickness, while in the coupled domain, WAVI solves for ice velocities and MITgcm solves for ice thickness and ocean properties, as described above. The coupled domain only needs to extend far enough inland to accommodate the grounding-line retreat occurring during a projection.

The coupled model solution procedure is split into coupling periods, chosen to equal the WAVI timestep of 20 days. Over each coupling period (Figure 1b) the following takes place: (1) WAVI calculates ice velocities over the whole ice domain for one 20-day timestep; (2) WAVI steps forward the ice thickness in the ice-only domain for one 20-day time step; (3) MITgcm receives the ice velocity for the coupled domain and the updated ice thickness on its boundaries, and sub-cycles the ice thickness and ocean properties within the coupled domain using the 200 s ocean timestep for the full 20 day coupling period; (4) MITgcm passes the new ice thickness for the coupled domain back to WAVI and the next coupling period commences.

For consistency, the same advection scheme that is used in WAVI (Arthern et al., 2015), has been coded into STREAMICE. Ice divergences are updated with the changing ice thickness in STREAMICE every ocean timestep, while the ice velocity remains fixed over each coupling period. We adopt the principle that the ocean may only melt ice that has no basal drag applied (Arthern and Williams, 2017), so the WAVI drag field is passed to MITgcm to decide where melting can occur during each coupling period. This means that no melting can occur on partially grounded cells, as recommend by Seroussi and Morlighem (2018). If, during a coupling period, a grid cell becomes grounded, melting on this cell is immediately switched off. In both the WAVI and STREAMICE models a minimum ice thickness of 50 m is applied.

Bedmachine version 3 is used as the basis for the bed/seabed geometry and initial ice thickness throughout the model. However, we found that without modification this dataset led to rapid grounding and advance of PIG. Closer inspection revealed that the seabed bathymetry may have been underestimated near the grounding line of this glacier in Bedmachine version 3 (Appendix B). Therefore, throughout the coupled domain we deepen the seabed wherever needed to achieve a minimum water column thickness of 280 m on velocity grid points over most of the domain, tapering towards grounded ice over 6 km down to a minimum water column thickness of 140 m. This procedure is only applied to cells with no ice basal drag in the initial state. This edited bathymetry is used in both MITgcm and WAVI.

https://doi.org/10.5194/tc-2023-77
Preprint. Discussion started: 9 June 2023

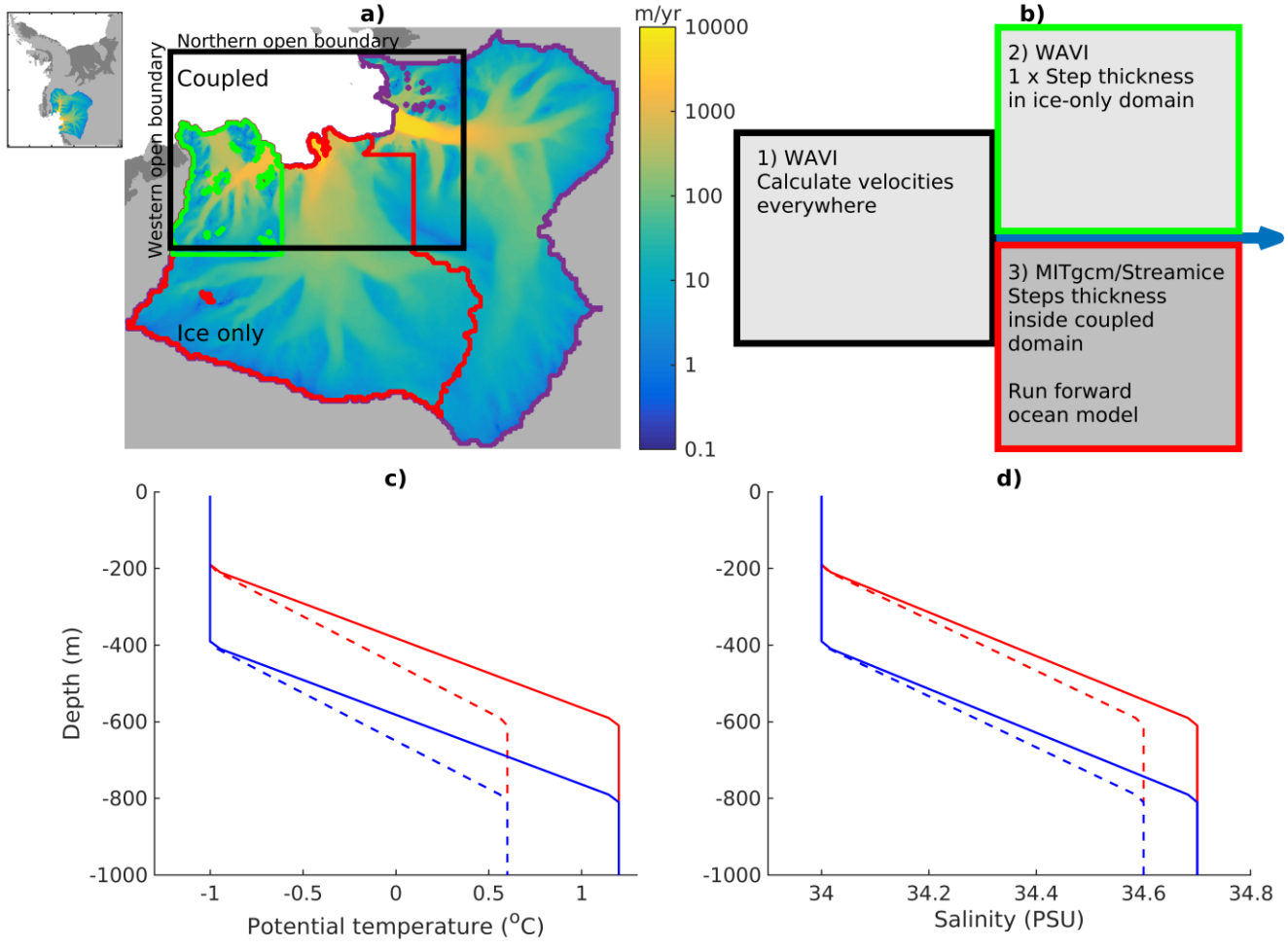

FIGURE 1: (a) Outline of the whole Amundsen Sea sector domain. The black box shows the outline of the coupled domain; the ice only domain is defined as everywhere outside of this box. The coloured regions represent the three regions used in analysis: PIG (purple), Thwaites (red), and Smith (green). (b) A schematic diagram of the three grouped steps of the coupled model applied during one coupling period. (c) Potential temperature boundary conditions for the Northern (solid line) and Western (dashed line) boundaries for the warm (red) and cold (blue) cases. (d) as in (c) but for salinity.

https://doi.org/10.5194/tc-2023-77
Preprint. Discussion started: 9 June 2023

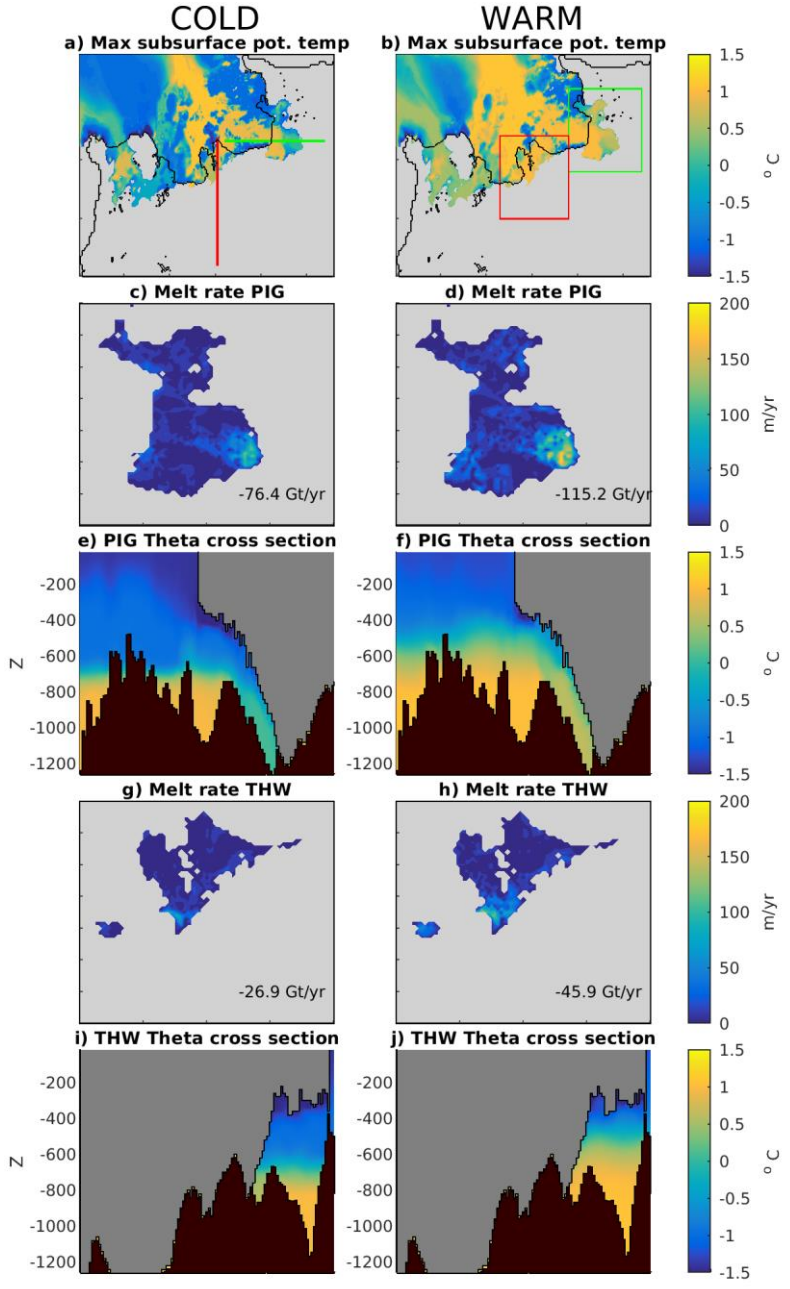

175 **FIGURE 2:** (a) Initial maximum subsurface potential temperature over the ice/ocean domain for cold case**. (**c) Initial melt rate over PIG Ice Shelf in the cold forcing case over the green box in (b). The label shows the total initial meltwater flux. (e) Cross-section through PIG Ice Shelf taken along the green line in (a) showing initial potential temperature in the cold case. (g) Initial melt rate over Thwaites Ice Shelf in the cold forcing case over the red box in (b). (i) Cross-section through Thwaites Ice Shelf taken along the red line in (a), showing initial potential temperature in the cold case. (e) (b), (d), (f), (h), (j), as in (a), (c), (e), (g), (i) respectively, but for the warm forcing case.

https://doi.org/10.5194/tc-2023-77
Preprint. Discussion started: 9 June 2023

180 **3 Results**

3.1 Amundsen Sea sector: 125 years simulation

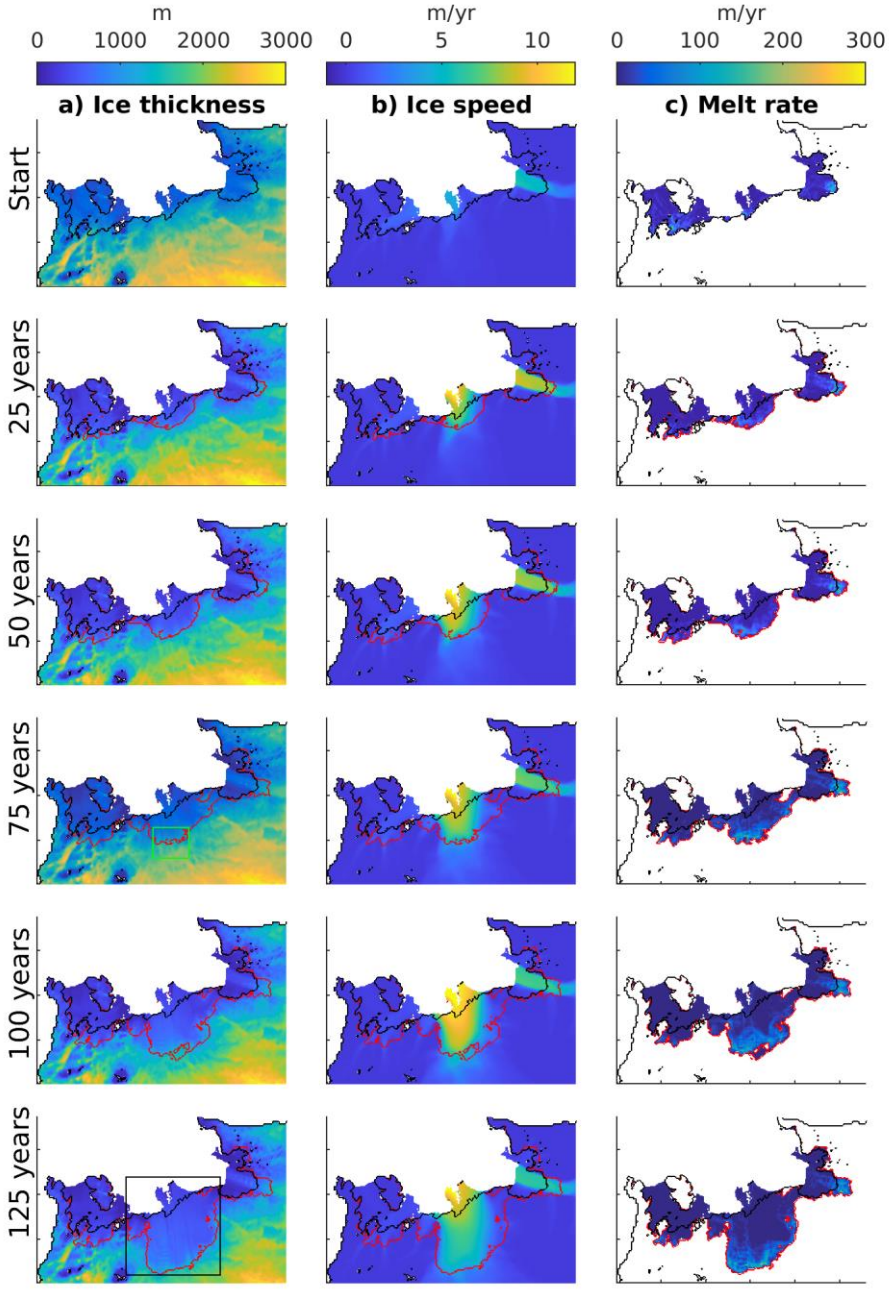

FIGURE 3: Warm forcing case evolution over 125 years. Panels show snapshots of (a) ice thickness, (b) ice speed and (c) melt rate, taken every 25 years throughout the simulation.

185

https://doi.org/10.5194/tc-2023-77
Preprint. Discussion started: 9 June 2023

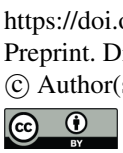

The Cryosphere Discussions

Following initialisation, the coupled ice/ocean model is run forward for 125 years under both forcing cases, as well as a zero-melting case. The evolution of the warm simulation is shown in Figure 3. The most prominent feature of the simulation is the acceleration (figure 3b) and grounding-line retreat of Thwaites Glacier (figure 3a). At the start of the simulation, Thwaites Ice Shelf hosts the observed fast-flowing western shelf and slower eastern ice shelf (figure 3b), where a pinning point restrains the flow of ice. However, as the simulation progresses, both sides of the ice shelf accelerate, reaching speeds of up to 12 km/yr. In addition, Thwaites Glacier experiences substantial grounding-line retreat during this simulation, leading to a reduction in the total mass of grounded ice and the formation of new larger ice shelf cavity, which features rapid melting rates (figure 3c). However, such trends in ice speed and grounding line retreat are restricted to Thwaites: neither PIG nor Smith Glacier experiences the same level of acceleration or retreat, although we do observe an initial acceleration of the PIG (which is later reversed), and some grounding line retreat in both PIG and Smith.

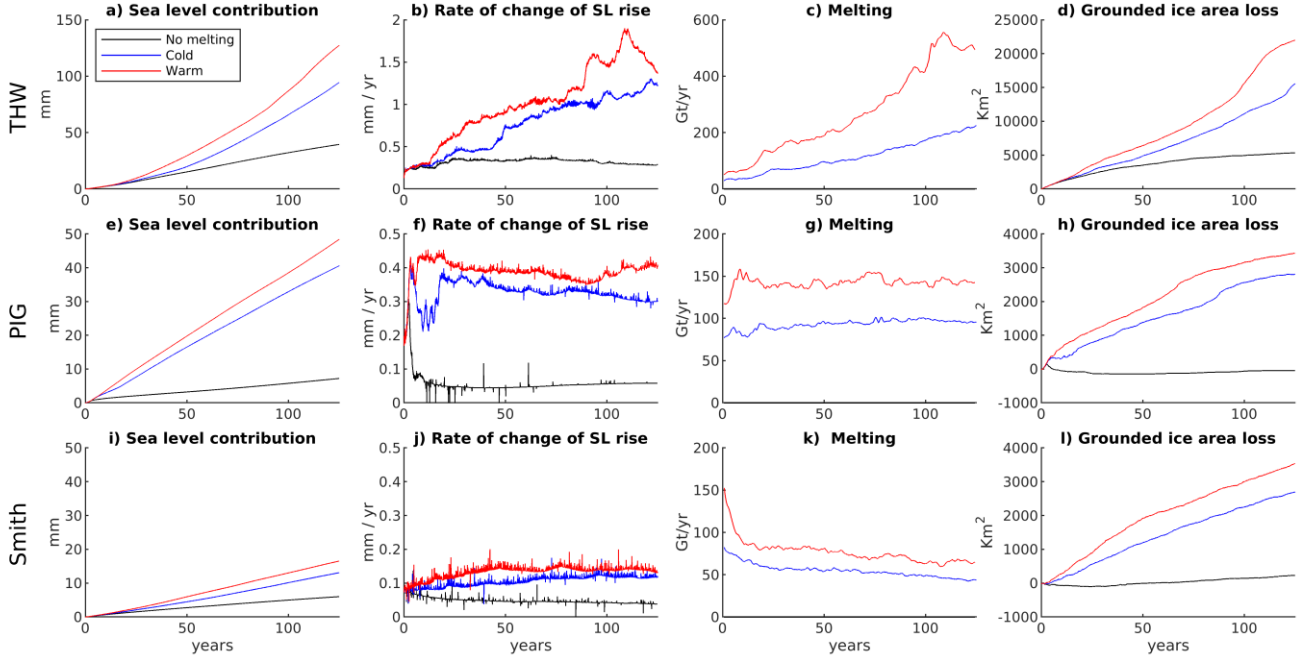

FIGURE 4: Timeseries shown for the three cases no melt (black line), cold (blue line), warm (red line). (a) Cumulative global sea level contribution from the Thwaites area. (b) Rate of change of global sea level contribution for Thwaites area. (c) Total ice shelf melt rate from the Thwaites area, with a 2-year running average applied. (d) Grounded area loss from the Thwaites area. (e) – (h) Same as above but for the PIG area. (i) – (l) Same as above but for the Smith area.

In order to analyse SLR contributions, melting and grounded ice area loss from different regions, and to compare the three forcing cases, we divide the domain into three areas: Thwaites, PIG and Smith (Figure 1a). The model projects notable SLR contributions from all three regions even in the zero-melting case, which has important implications. This result demonstrates that the initialised ice-sheet state in WAVI is intrinsically unsteady and will continue the present-day ice loss for some period

https://doi.org/10.5194/tc-2023-77
Preprint. Discussion started: 9 June 2023

of time irrespective of future climatic forcing. This implies that a tipping point may have been passed at some point, likely during the 20th century (Mouginot et al., 2014), and some amount of SLR (at least ~50 mm in our simulations) is now committed. Zero melting can never occur in the real world, because even seawater at the surface freezing point will drive melting at depth due to the pressure decrease in the freezing temperature, so this is a very conservative test of the presence of committed ice change. However, the contribution from PIG is dependent on the particular choice of bathymetry deepening that is implemented (Appendix B). Notably, we observe the largest zero-melting SLR contribution from the Thwaites area, leading to ~40 mm in 125 years, with a near constant SLR rate. For the Thwaites area we also obtain some grounding line retreat, though the rate of loss reduces during the simulation, suggesting that the SLR contribution would stabilise after a further period of simulation.

The cold and warm cases are far more realistic since they are based on observed Amundsen Sea conditions. Both scenarios contribute much more SLR than the zero-melting case (figure 4a, e, i). In both cases, the Thwaites area dominates SLR contributions from the sector, providing approximately two-thirds of the total, and responds differently to melting than the PIG and Smith areas. In PIG and Smith areas, the rate of SLR with melting is approximately constant, but obtains higher rates of SLR than in the zero-melting case, increasing to ~0.4 mm/yr and ~0.1 mm/yr, in the warm case, respectively, (figure 4f, j). However, in the Thwaites area with melting a trend emerges in the SLR rate (figure 4b), increasing from 0.2 mm/yr at the start of the simulation to ~1.5 mm/yr at the end, in the warm case. In addition, we observe rapid jumps in the SLR rate for Thwaites that are not present in the other areas. The increase in the SLR rate in the Thwaites results in an approximately quadratic SLR contribution (figure 4a), rather than the more linear SLR contributions obtained for PIG and Smith. In addition, we observe an increase in the total melting that occurs from the Thwaites Ice Shelf as the simulations progresses: over the 125 years of the simulation, the total melt flux from Thwaites increases by an order of magnitude, from 50 (20, respectively) Gt/yr at the start of the simulation to over 600 (200) Gt/yr at the end in the warm (cold) case (figure 4c), which occurs despite constant oceanic boundary forcings during the simulation. In the PIG and Smith areas, the total melt flux is approximately constant (figure 4g, k). However, we do observe a strong correlation between the cumulative integral of melting and the SLR contribution individually for each region (Appendix C).

For all regions, we obtain consistently higher SLR rates and grounded ice area loss in the warm forcing case compared to the cold forcing case (figure 4b, f, j). However, as a fraction of the total SLR in these models, the difference between warm and cold scenarios is remarkably small, only ~25%, by the end of the simulations. Given that these scenarios bracket the coldest and warmest ocean conditions on record in the Amundsen Sea, this suggests that the future SLR from this region is only weakly influenced by variations within the plausible range of ocean conditions: while melting is important to the SLR, its typical climatic variations are less so. Despite this, in the Thwaites area we observe different timings and strengths in the jumps in the SLR rate between the cold and warm cases (figure 4b). We also observe an increasing difference between the cold and warm

https://doi.org/10.5194/tc-2023-77
Preprint. Discussion started: 9 June 2023

total melt rates for Thwaites Ice Shelf (figure 4c), while for the PIG and Smith areas this difference remains approximately constant (figure 4g, k).

Overall, we conclude that melting and SLR have a fundamentally different response in the Thwaites area than the other areas, leading to an increasing SLR rate and total melting rate. In addition, the Thwaites area dominates the SLR contribution for the Amundsen Sea sector over the 125 years simulated. Therefore, the remainder of this study focusses upon the processes underlying this behaviour in the Thwaites area.

3.2 Thwaites Glacier retreat and ice shelf pinning points

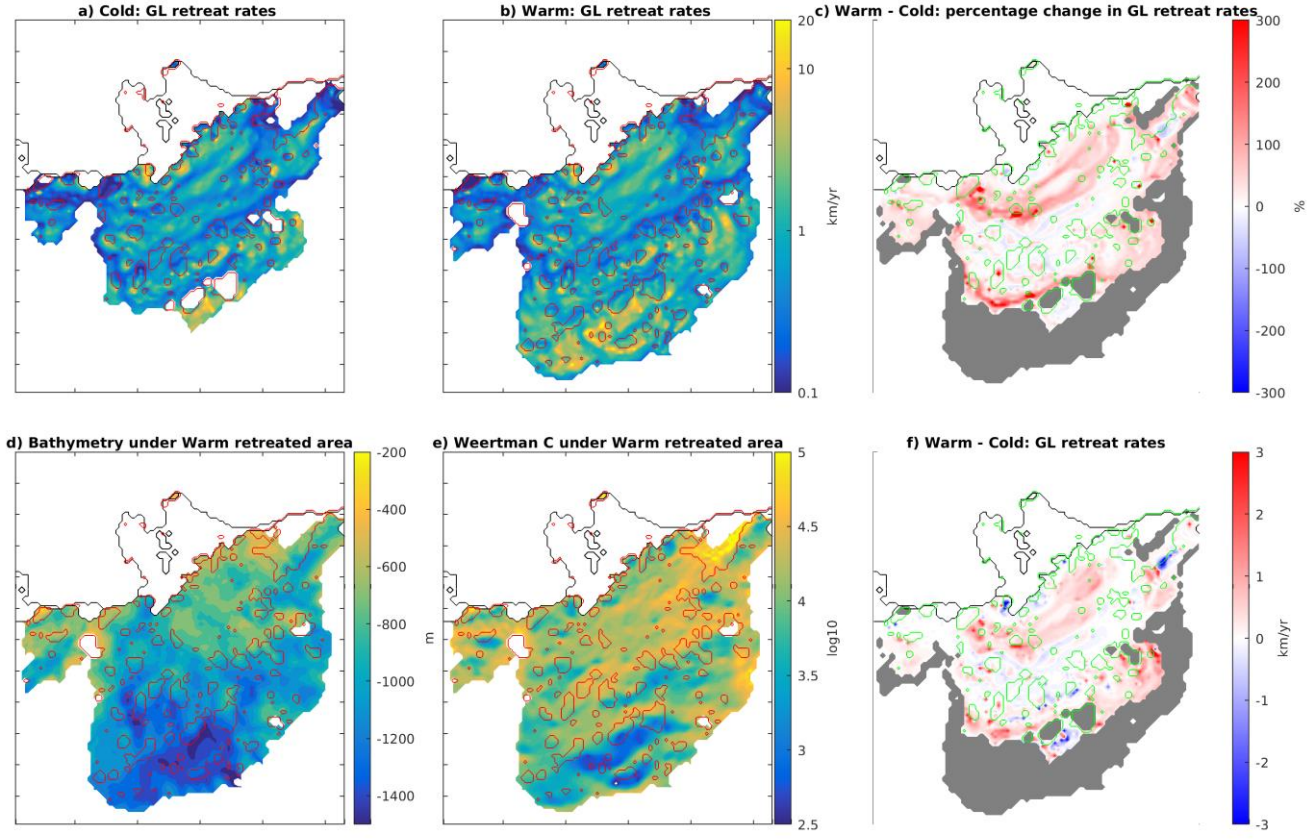

FIGURE 5: (a-b) Grounding line retreat rates over the 125 year simulations in the cold (a) and warm (b) indicated by colours, with colour bar shown in (b). In each the red contours show the presence of an isolated pinning point during the simulation. (c) Percentage change in grounding line retreat rates between the cold and warm cases (i.e., the percentage difference between those retreat rates shown in (a) and (b)

https://doi.org/10.5194/tc-2023-77
Preprint. Discussion started: 9 June 2023

respectively). (d-e) Bathymetry (d) and Weertman C coefficient (e) in the final extent of the grounding line retreat in the warm case. (f) The difference in grounding line retreat rates between the cold and warm cases (colours) as well as final grounding line area (grey area). The area shown in each panel corresponds to that displayed as a black box in Figure 3.

Figure 5 shows quantities related to Thwaites grounding line retreat, which is one of the key features that differentiates this area from the PIG and Smith areas. Over the simulation, the warm case has a larger area of grounding-line retreat than the cold case, with a faster rate on average (figure 5 a, b, c, f). Grounding line retreat rates are calculated from the discrete migration of the grounding line across grid cells. Specifically, the retreat rate in each grid cell is calculated as $\Delta x_{GL} / \Delta t_{GL}$, where Δt_{GL} is the time between when the subject cell first becomes a grounding line cell (any of the 8 adjacent cells are floating) to when that cell ungrounds, and Δx_{GL} is the grid cell width or diagonal extent depending on which adjacent cell was first floating. Figures 5d and 5e show the bed depth and 'Weertman C' basal drag coefficient over the area of grounding-line retreat in the warm case (the fields are the same in the cold case). A lower Weertman coefficient corresponds to a more slippery bed. In both warm and cold cases, highly heterogeneous retreat rates are observed (figure 5a, b), with areas of fast retreat as high as 20 km/y in proximity to areas of much slower retreat. Towards the end of the warm case simulation, the grounding line experiences rapid retreat (Figure 5b) across a deep and slippery bed section (Figure 5d-e) before slowing down as it encounters a ridge of shallower and less slippery bed. These features explain the large variations in the Thwaites area SLR rate in the last 40 years of the simulation (Figure 4b).

Comparing the cold and warm scenarios we see the effect of increased melting on grounding-line retreat rates. More specifically, we observe areas of elevated grounding line retreat rate in the northern part of the ungrounding area, below which an area with minimal sensitivity to melting scenario, and again by increased rates in the south (Figure 5f). There are very large percentage increases in grounding-line retreat rates for these two clear bands on the retreated area (Figure 5c).

In addition, we observe the formation of many pinning points as Thwaites Glacier retreats, shown by red and green contours in Figure 5 for the different cases. An ice grid cell is flagged as a 'pinning point' if it is grounded but separated from the main grounded ice sheet by floating ice. The red/green contour is then drawn around all cells that are flagged as pinning points in any one of the outputs. The pinning points are generally located on areas of shallow bathymetry that are downstream of areas of deeper bathymetry (Figure 5d). The pinning points typically feature slower retreat rates, and inshore of these pinning points we generally observe areas of faster retreat (Figure 5a, b). These pinning points are crucial for the future evolution of Thwaites Glacier, as they provide drag and buttressing as the ice retreats. The importance of these pinning points is determined by their size, position, and duration, so we examine these features and their relationship to SLR rates from the Thwaites area.

https://doi.org/10.5194/tc-2023-77
Preprint. Discussion started: 9 June 2023

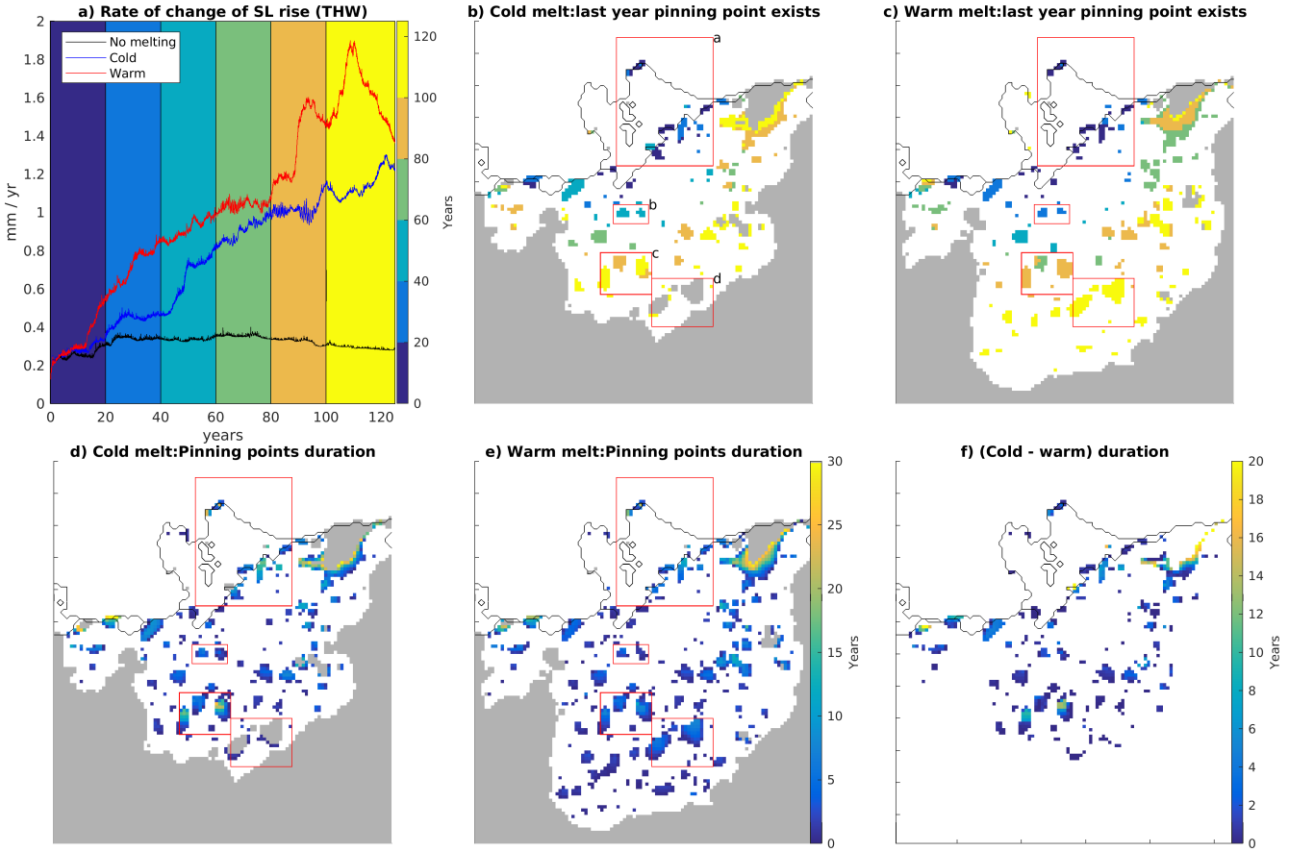

FIGURE 6: (a) SLR contribution rates for Thwaites area for warm (red), cold (blue) and no melt (black) cases. The background colour indicates the time in the simulation according in bands of 20 years. (b) Colours indicate the band of the final year that pinning point cells exists for cold melt case, according to the colours shown in (a). Note that only pinning points that exist for over 1 year are shown. Red labelled boxes refer to groups of pinning points discussed in the text. (c) Same as (b) but for warm case. (d-e) Pinning point duration, taken as the time from isolation to ungrounding, for cold (d) and warm (e) cases. (f) Difference in pinning point duration between cold and warm cases (i.e. the difference the data shown in d and e), where pinning point locations match. In (b)-(e), grey regions indicate areas which do not become ungrounded during the simulation. The Area shown in Figures b-f is shown in Figure 3 as a black box.

Figure 6b-c shows the ungrounding time of pinning points in the cold and warm cases, respectively. By examining these times, we can compare how the ungrounding of pinning points relate to jumps in SLR rate that we observe from the Thwaites area. The labelled red boxes in Figure 6b show the key groups of pinning points in the simulations.

https://doi.org/10.5194/tc-2023-77
Preprint. Discussion started: 9 June 2023

Within the first 20 years, the SLR rates of the warm and cold forced cases diverge (Figure 6a). In the warm case, pinning point group 'a' completely ungrounds between years 10 and 20 (Figure 6c), with the removal of the associate buttressing leading to a large jump in SLR rate; However, in the cold simulation, extra pinning points exist in this group and some of these pinning points remain grounded until beyond 40 years (Figure 6b), leading to a period of steady SLR rate in this simulation (Figure 6a). The final ungrounding of this group's ('a') last pinning point coincides with the ungrounding of group 'b', leading to the large jump in SLR rate in the cold simulation after 40 years. In the zero-melting case, part of pinning point group 'a' and all of 'b' remain grounded throughout the simulation (not shown), and SLR rates remain approximately constant as a result (Figure 6a). In the warm simulation, group 'c' becomes ungrounded by 90 years, causing a rapid increase in SLR rate, and the loss of group 'd' at 110 years leads to another large jump. The cold simulation loses group 'c' at 120 years, leading to a small jump in SLR rate, while group 'd' remains grounded at the end of the simulation.

Figure 6d-e shows the duration of the pinning points; the time between separation from the main body of grounded ice to ungrounding. There is a large variation in pinning point durations, with some lasting less than a year while others persist for decades. In general, the duration of pinning points is lower in the warm case (Figure 6d-f), leading to the different ungrounding times and SLR rates as described above. Reducing the duration of pinning points increases the length and intensity of periods of rapid ice acceleration.

https://doi.org/10.5194/tc-2023-77
Preprint. Discussion started: 9 June 2023

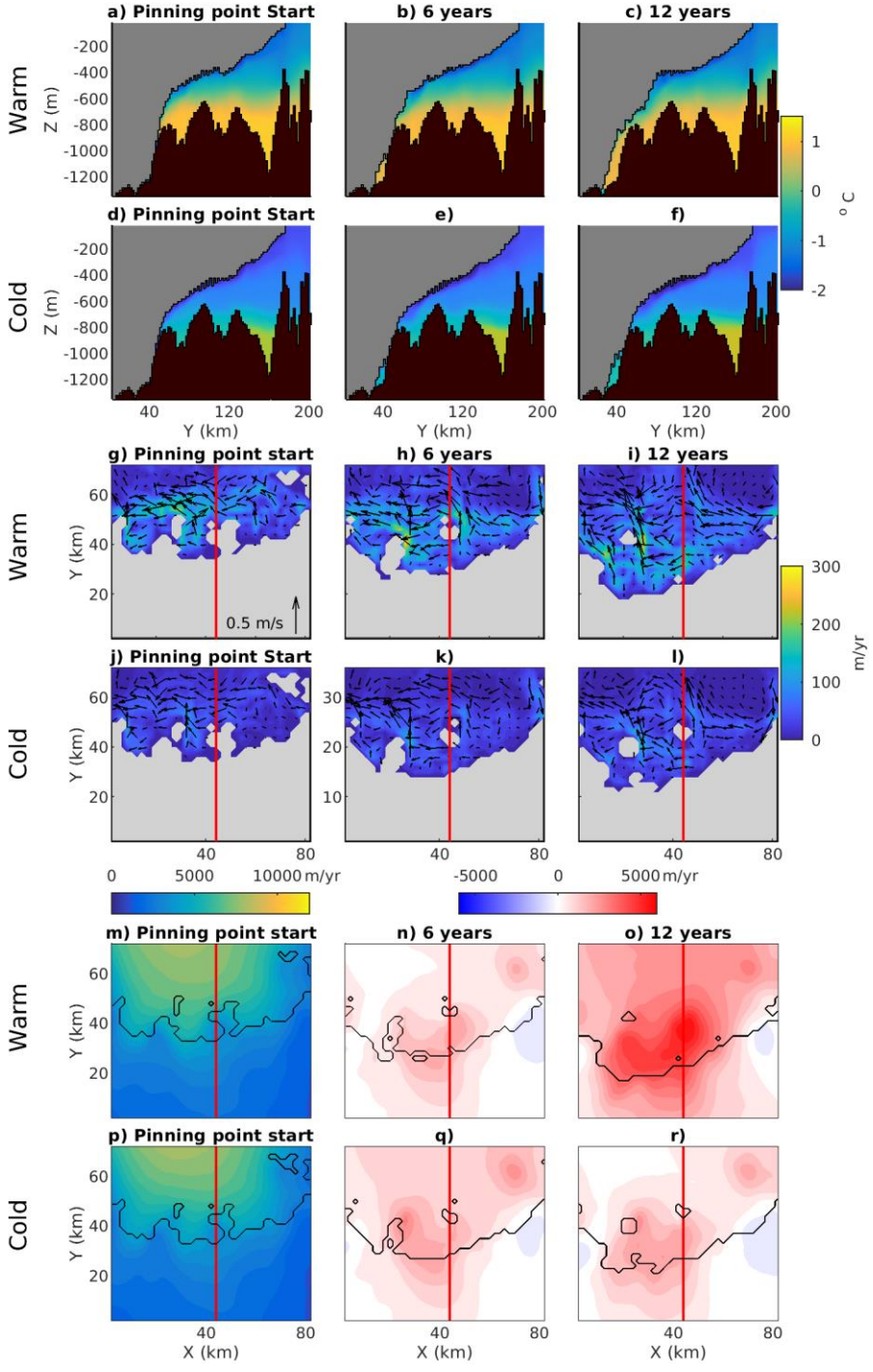

FIGURE 7: Snapshots every 6 years starting from the date of group 'c' pinning point formation in the warm and cold cases (79 and 94 years respectively). (a-c) Cross section through the Thwaites Ice Shelf, taken along the red line in (g) extended to ice front, for warm case. (d-f) Same as (a-c) but for cold case. (g-i) Melt rates for warm case, with arrows showing ice shelf boundary layer ocean velocities (j-l) Same as

https://doi.org/10.5194/tc-2023-77
Preprint. Discussion started: 9 June 2023

(g-i) but for cold case. (m) Ice speed snapshots at start of pinning point formation and (n, o) show differences for warm case. (p-r) Same as (m-o) but for cold case. Area shown in (i-x) is shown in figure 3 as a small green box.

To illustrate the key role of pinning points, we now focus on the ungrounding of group 'c', which causes the rapid jump in SLR rate at year 90 in the warm simulation, and the smaller jump at year 120 in the cold simulation. Figure 7 shows the evolution of the two simulations, starting from their individual dates of formation of the group 'c' pinning points. Figures 7a-l show ice geometry and ocean conditions throughout the subsequent evolution. To begin with, the grounding line is located in shallower bathymetry at the top of a retrograde slope (figure 7a, d). Ungrounding then occurs laterally around this point, including upstream, encircling the pinning point and leaving it isolated from the rest of the grounded ice (figure 7h, k). Note that the pinning point is grounded on the side of the shallower bathymetry, rather than on top of the bathymetric feature. With the grounding line now in a deeper bed an acceleration is expected, although the pinning point continues to provide basal drag that resists the flow. The advection of thicker ice from the deeper bed upstream enables the ice to remain grounded on the shallower bed beneath the pinning point. Therefore, only a small acceleration is observed at 6 years, while the ice remains grounded on the pinning point (Figure 7m-r).

However, melting now occurs in the newly-opened cavity upstream of the pinning point. This thins the ice, enlarging this cavity, enabling greater oceanic connection, and leading to higher ocean velocities and melt rates (figure 7h, k). This melting and thinning feedback eventually leads to sufficient thinning upstream of the pinning point for it to unground completely (Figure 7i). The resultant loss in buttressing leads to a large increase in ice speed (figure 7o), further rapid grounding line retreat and a jump in SLR rate. Therefore, the distribution and strength of localised melt rate patterns strongly determines the duration of these pinning points and thus the overall ice retreat. This is shown clearly in Figure 7g-l, with the warm case leading to higher melt rates and a much faster ungrounding of the pinning point. The melt rates around these pinning points are highly heterogeneous (Figure 7g-l), with elevated melt rates typically occurring on their eastern side, where rapid ocean currents drive high melt rates. These rapid currents occur where buoyancy-driven meltwater flow is trapped against the grounding line by Coriolis force (Holland and Feltham, 2006).

https://doi.org/10.5194/tc-2023-77
Preprint. Discussion started: 9 June 2023

3.3 Thwaites Ice Shelf geometric melting trends

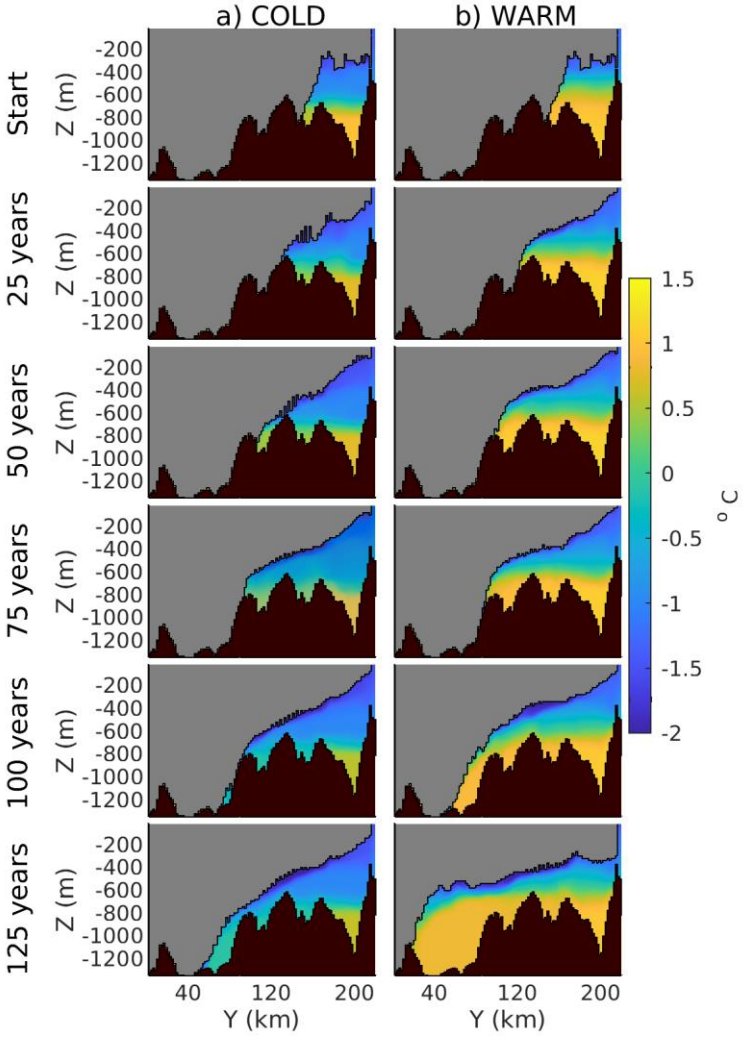

FIGURE 8: Cross sections of potential temperature beneath Thwaites Ice Shelf for warm (top) and cold (bottom) cases, along the same section as shown in Figure 7 and Figure 2i, j, which is, represented in Figure 2a as the red line.

An increasing trend in the total ice shelf melting occurs over the evolving Thwaites Ice Shelf, during both the warm and cold forcing simulations (Figure 4c). The wider oceanic forcings are fixed, so these trends must be driven by geometric changes in the ice shelf cavity. In Figure 8 we show how the Thwaites cavity geometry and ocean conditions evolve in the two cases. The warm case has a higher thermocline, so the warm CDW is more easily able to flow over ridges and flood the new cavity areas. In the cold case, the access of the warmest CDW is blocked by seabed highs, with only more modified CDW reaching the ice base. However, sufficiently warm water is still able to drive melting close to the grounding line. In both cases the ice base near the grounding line remains steeply sloped throughout the retreat.

https://doi.org/10.5194/tc-2023-77
Preprint. Discussion started: 9 June 2023

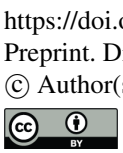

Figure 9a shows the evolution of total melt flux from the Thwaites Ice Shelf in the warm case, for both the entire ice shelf and for ice below 600 m depth only, which is the thermocline depth in this case. Most of the trend in ice shelf melting occurs in the deeper ice, with melting below 600 m peaking at an increase of ~30 times its initial value, which suggests that as the grounding line retreats, a strong increase in ice shelf base area below the thermocline controls total melting (Figure 9b). This increase in deep ice area occurs because the groundling line retreats into deeper bathymetry, but also because the slope of the ice shelf base gets shallower during the simulation, as shown for example in Figure 8. Without an increasing trend in melt flux, the thicker ice advected across the grounding line as the ice sheet retreats into deeper bathymetry would result in re-grounding on pinning points further downstream. The close correspondence in the increase between total melting (Gt/yr) and ice base area (km^2) implies that the average melt rate (m/yr) beneath deep ice is approximately constant (Figure 9c). However, we do find some temporal variability in this average melt rate, and importantly the local melt rates are highly variable, with a spatial standard deviation close to the mean value. This spatial variability is important for the effect of melting on small scale pinning points, as described above.

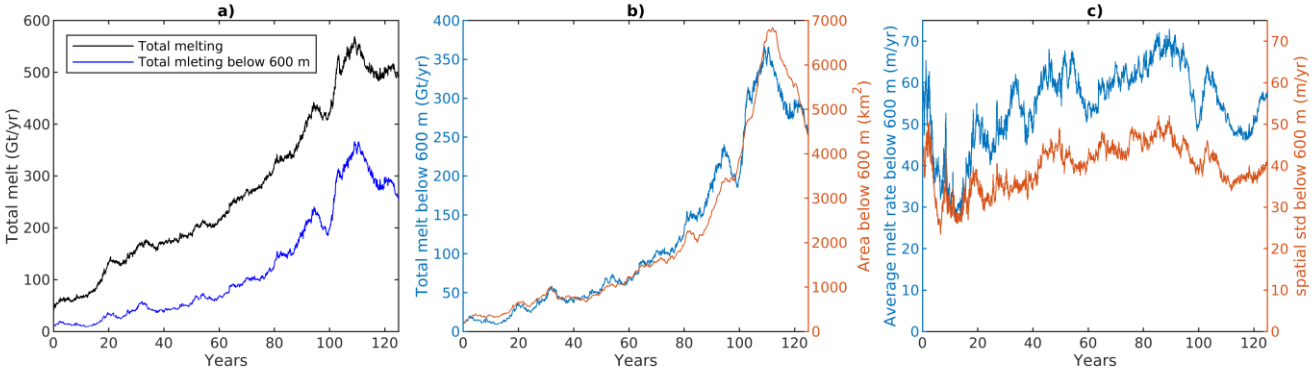

FIGURE 9: (a) Total melt flux from the full Thwaites Ice Shelf area (black) and from grid cells located below 600 m depth only (blue). (b) Total melt flux from grid cells below 600 m and total ice area below 600 m. (c) Average melt rate on grid cells located below 600 m depth and spatial standard deviation of these melt rate values.

4 Discussion

This study considers the future evolution of ice streams in the Amundsen Sea sector using a coupled ice/ocean model. Under both warm and cold forcing we find large grounding line retreat and ice acceleration from Thwaites Glacier, with the Thwaites area dominating future SLR contributions from the region. The SLR from the Thwaites area is consistent with a previous coupled model study (Seroussi et al., 2017), which considered a shorter time span of 50 years. In this study however, we show

https://doi.org/10.5194/tc-2023-77
Preprint. Discussion started: 9 June 2023

a larger sensitivity to a realistic range of ocean forcings, in the shorter and longer term, and an increasing SLR rate, which continues over the 125 year time period, from the Thwaites area. This was not observed in previous coupled modelling of Thwaites Glacier (Seroussi et al., 2017), although it was observed in some ice-only simulations, depending on uncertainty in ice dynamics (Nias et al., 2019) and uncertainty in melt rates (Arthern and Williams, 2017). A previous ice-only study has set 1 mm/yr SLR rate to be the threshold that implies rapid retreat and collapse of Thwaites glacier (Joughin et al., 2014), and this is exceeded sooner in our simulations, within 100 years. However, our simulations are not long enough to see how the full implications play out over multiple centuries.

In our simulations, the increase in SLR rate from the Thwaites area is caused by ocean-driven melting, and the magnitude of this increase is sensitive to different rates of melting in warm and cold scenarios. The SLR rate is governed by a balance between retreat of the grounding line into deeper bed regions, and the formation and duration of pinning points during this retreat. Crucially, this study shows the importance of ocean-driven melting in ungrounding these pinning points, reducing ice-shelf buttressing and enhancing grounding-line retreat. It should be noted that the modelled rates of ungrounding upstream of pinning points are high enough to explain recent observations (Graham et al., 2022). Other studies have hypothesised about the mechanics and importance of pinning points (Thomas, 1979), and have shown the effect of pinning points in an idealised ice/ocean coupled model (De rydt and Gudmundsson, 2016). In this study we clearly show the importance of these mechanisms in a synchronous coupled model of the future Thwaites Ice Shelf. The importance of future pinning points suggests the need for more accurate knowledge of bathymetry and bed properties in the grounded portion of Thwaites Glacier, as well as highlighting the importance of accurately modelling the effects of pinning points in both ice sheet and ocean models. We have shown that high resolution coupled ice-ocean models are required to investigate the effect of pinning points on ice dynamics.

One important question raised by our study is why Thwaites Glacier appears to behave differently from the other glaciers in the region. We speculate that this is caused by the wide trunk of this glacier. As the grounding line of the Thwaites Glacier retreats it forms an extremely short and wide ice shelf, unlike the other glaciers in the region, whose ice shelves are confined within embayments. As a result, the buttressing provided by lateral ice shelf margins is very weak for Thwaites Glacier; this also explains the high sensitivity to pinning points which therefore provide the majority of the buttressing of Thwaites. Therefore, while a recent study found that Thwaites Ice Shelf provides limited buttressing in the present day (Gudmundsson et al., 2023), we find that future configurations of Thwaites Ice Shelf will provide important buttressing, as its groundling line retreats. The dependence of this future buttressing on ocean forcings will determine the future SLR from this sector.

One of the limitations of this study is that steady, idealized, ocean forcings are applied to the northern and western boundaries. However, ocean conditions in the region are known to have strong decadal variability (Jenkins et al., 2018; Dutrieux et al., 2014). Some of the pinning points only exist for ~10 years, so decadal variability in oceanic forcings may have an important role in how quickly these pinning points are ungrounded. In addition, a superimposed anthropogenic warming trend in ocean

https://doi.org/10.5194/tc-2023-77
Preprint. Discussion started: 9 June 2023

forcing may be expected in the Amundsen Sea (Holland et al., 2022; Naughten et al., 2022), which could decrease the duration of future pinning points and speed up the retreat of Thwaites Glacier. Another limitation of this study is the use of an ocean model that does not represent the evolution of oceanic conditions and sea ice on the wider Amundsen Sea continental shelf. As such, our model might lack important feedbacks such as increased ocean currents driven by ice-shelf meltwater bringing more CDW onto to shelf and driving higher melt rates (Kimura et al., 2017; Jourdain et al., 2017; Donat-Magnin et al., 2017). In addition, the oceanic simulation lacks the physical presence and effect of freshwater sources, like sea ice and icebergs, which impacts oceanic currents and the delivery of warm CDW to the base of ice shelves in the region (Bett et al., 2020). With an order of magnitude increase in ice shelf melting in our projections, such feedbacks would be substantial.

The simulations show how the geometric changes in the Thwaites Ice Shelf and its cavity can lead to an increasing ice area at depth, meaning that more of the ice base is exposed to deep warm waters and leading to an increasing trend in total melt flux. Although this general depth dependence on melting is often captured by parametrizations of melting (Asay-Davis et al., 2017), we have shown that there is strong spatial variability in melting, and this spatial variability has important consequences for pinning point duration. The increasing trend in total melt rates is needed to maintain the ice retreat, as it counteracts increased ice thickness advection across the grounding line, which would otherwise ground the ice on bathymetry further downstream.

A key limitation of the model used in this study is the lack of ice shelf calving-front retreat, which could impact the ice dynamics and total melting (e.g. Bradley et al., 2022; Joughin et al., 2021). In addition, the model lacks an evolving damage field impacting ice dynamics (Lhermitte et al., 2020). However, we believe that these limitations cause our simulations to be a conservative estimate of Thwaites Glacier retreat, as calving and evolving damage are only expected to enhance the retreat. Barring the existence of major calving- or damage-driven ice retreat over the next 125 years, our results suggest that the ocean-driven ungrounding of pinning points will dictate the future SLR from the Amundsen Sea sector. However, strong sensitively of ice-sheet projections to basal friction laws provides uncertainty to modelled ice retreat rates and mass loss, with the Weertman sliding law used in this study found to systematically predict the lowest ice mass losses (Brondex et al., 2019; Cornford et al., 2020). It should also be noted that uncertainties in the accumulation field and that it is fixed in this study could potentially affect the modelled ice dynamics.

5 Conclusions

This study presents, for the first time, 125-year predictions of ice evolution in the Amundsen Sea sector of the West Antarctic Ice Sheet using a new synchronously coupled ice/ocean model, which includes full mass conservation in the coupled ice/ocean system, and an instantaneous response of melt rates to the evolving ice geometry. The coupled simulations were forced with idealised warm and cold ocean conditions in the wider Amundsen Sea, and compared to each other, as well as to a zero ice-shelf melting case.

https://doi.org/10.5194/tc-2023-77
Preprint. Discussion started: 9 June 2023

Even in the zero-melting case, the model predicts that all glaciers in the region lose ice mass during the simulations. This implies that the ice sheet model is initialised into an intrinsically unsteady state, so that a tipping point may have occurred in the past and we are now committed to further sea-level rise from this sector. However, when melting is activated in the coupled model, the rates of ice loss are much higher. This implies that ocean melting plays an important role in the future SLR contribution from this sector, though the difference between warm and cold scenarios is relatively modest, at only ~25% of the total SLR.

For the Pine Island and Smith Glaciers, the rate of SLR remains relatively constant throughout the projections, leading to a linearly-increasing sea-level contribution. The Thwaites Glacier area provides a much larger sea-level contribution, and features an increasing SLR rate, which causes its sea-level contribution to increase approximately quadratically with time. The rate of SLR from Thwaites Glacier is closely controlled by the formation and duration of isolated pinning points during the retreat of its grounding line. Ocean-driven melting is crucial in driving the ungrounding of these pinning points, by thinning the ice upstream, and this is the key mechanism by which future ocean conditions affect the SLR from this sector.

The coupled simulations show a large geometry-induced increase in total ocean-driven melting as Thwaites Glacier retreats and its ice shelf enlarges. This increased melting counteracts ice shelf thickening associated with thicker ice being advected across the deeper grounding line, which would otherwise cause the ice to ground downstream and arrest the retreat. Our simulations indicate large spatial and temporal variability in the melt rates. This variability will not appear within simple melting parameterisations.

Our results also suggest that accurate modelling of ocean-driven melting and ice response around pinning points, and accurate characterisation of the bed geometry and properties that lead to the formation of pinning points must be future research priorities. In addition, the further development and application of coupled ice/ocean models must be a priority, as it is difficult to envision how many of these results could have been achieved with parameterised ocean-driven melting.

Appendices

Appendix A: Ice shelf melt rate tuning

In the initial setup of the ice model, we can calculate the implicit melt rate (IMR), which is the melt rate required to recreate observed present day surface elevation changes in the ice model, given initial ice model velocities and geometry (Arthern and Williams, 2017). In this model, we attempt to minimise initial coupling shock by reducing the mismatch between the ice model IMR and the initial ice shelf melting field calculated from the MITgcm ocean model. To do so, we tune the ice shelf drag coefficient in the three-equation formulation of melting parametrisation used in the MITgcm (Jenkins et al., 2010). We found

https://doi.org/10.5194/tc-2023-77
Preprint. Discussion started: 9 June 2023

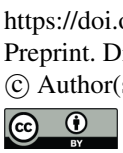

that a choice of drag coefficient of 0.01 minimises the combined PIG and Thwaites ice shelves mismatch in total melt flux (Figure A1), while average ocean forcings are applied, with the thermocline placed at 700 m depth.

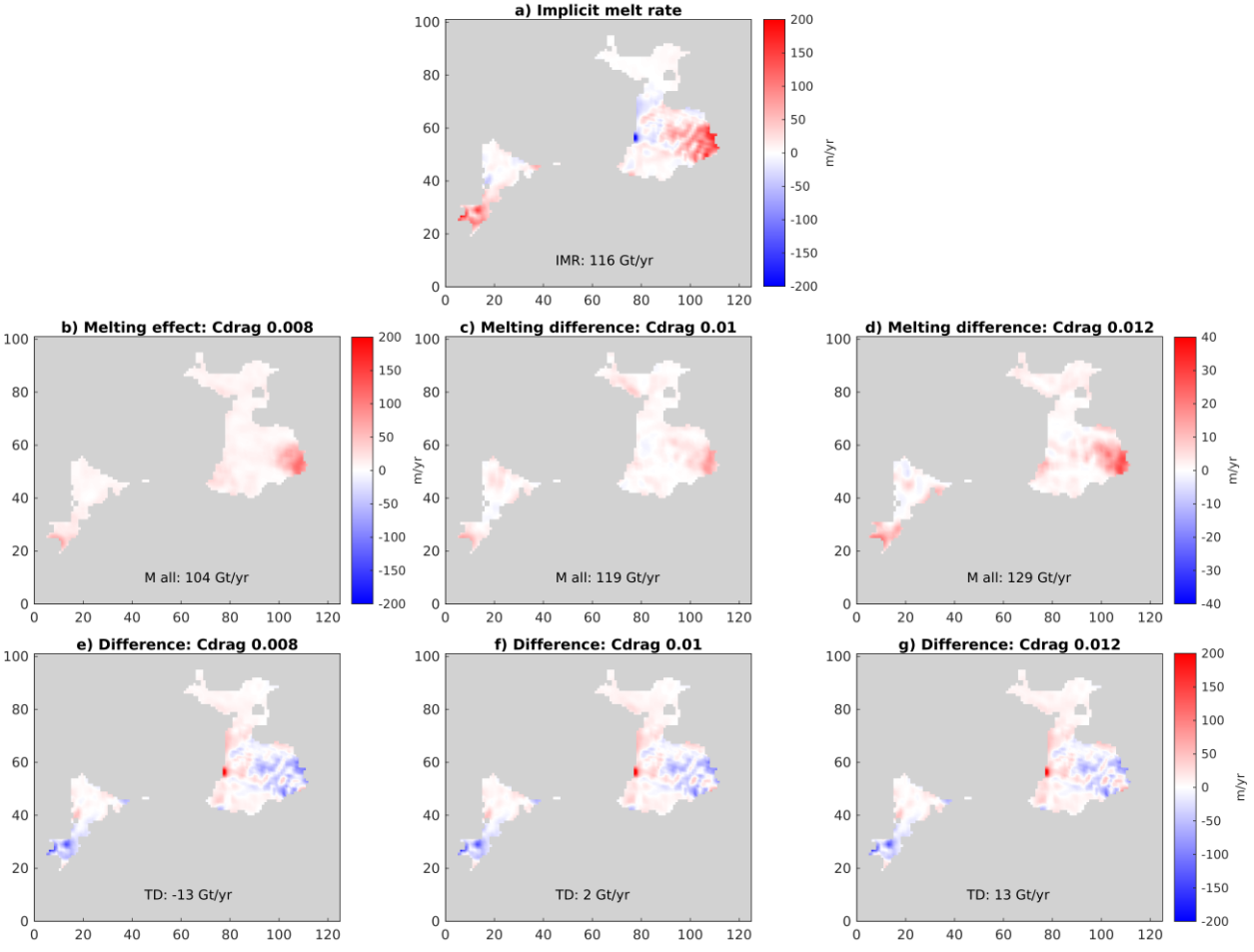

FIGURE A1: Area shown for PIG and Thwaites ice shelves. a) Initial implicit melt rate from the WAVI ice sheet model. b) Initial ice shelf melt rate from the MITgcm model for different values of the drag coefficient as follows (and labelled): 0.008 (b), 0.01 (c), and 0.012 (d), where (c), (d), shown as the difference from (b). (e-g) Difference between initial implicit melt rate and initial ice shelf melting for the MITgcm model melt rates shown in panels (b)-(d) respectively.

Appendix B: Initial bathymetry digging

To ensure the bathymetry field from BedmachineV3 (Morlighem et al., 2020; Morlighem, 2022) has a specified minimum water column thickness on velocity grid points, we performed a `digging' procedure, in which the bathymetry in areas with a water column thinner than a specific value is artificially deepened. This procedure was applied only to grid cells in which no

https://doi.org/10.5194/tc-2023-77
Preprint. Discussion started: 9 June 2023

ice drag is applied in the initial state. We found this step is necessary because, without it, the PIG Ice Shelf cavity has an excessively thin water column near the grounding line. This leads to minimal ice shelf melting in this region (Figure B1c), which leads to a large mismatch with the calculated initial IMR (Figure A1). This, combined with the shallow bathymetry, leads PIG to reground immediately at the start of the simulation, resulting in unrealistically low SLR rates from this region (Figure B1d).

Therefore, digging was applied in order to prevent re-grounding and minimise any changes in SLR rate at the start of the simulation (Figure B1d). However, enforcing a uniform minimum water-column thickness everywhere would create a sudden step-change in the bathymetry at the grounding line. Therefore, a taper is applied to the water column thickness used in the digging procedure, increasing the minimum thickness from a low value at the grounding line to its standard value over 6 km distance. After applying the digging procedure, PIG does not reground at the start of the simulation. However, we note that in the set up used in this study (280 m minimum thickness tapered to 140 m at the grounding line), there is a rise in the SLR rate from PIG at the start of the simulation, so that it no longer matches the observed value used in the model initialisation (figure B1d). This rise does not occur in a test simulation where the ice shelf melting is fixed to its initial value, with zero melting on newly ungrounded cells. This suggests that this rise in SLR rate is caused by feedbacks associated with melting on newly ungrounding cells. We note that the initial SLR rate from the Thwaites region (Figure B1a) is unaffected by the digging procedure. While the digging of the PIG water column is somewhat subjective, the deeper water column better reflects the sparsely available observations of the cavity near the grounding line (Dutrieux et al., 2014). Overall, the necessity of digging emphasises the importance of obtaining more detailed observations of the geometry of ice shelf cavities, beneath PIG in particular.

https://doi.org/10.5194/tc-2023-77
Preprint. Discussion started: 9 June 2023

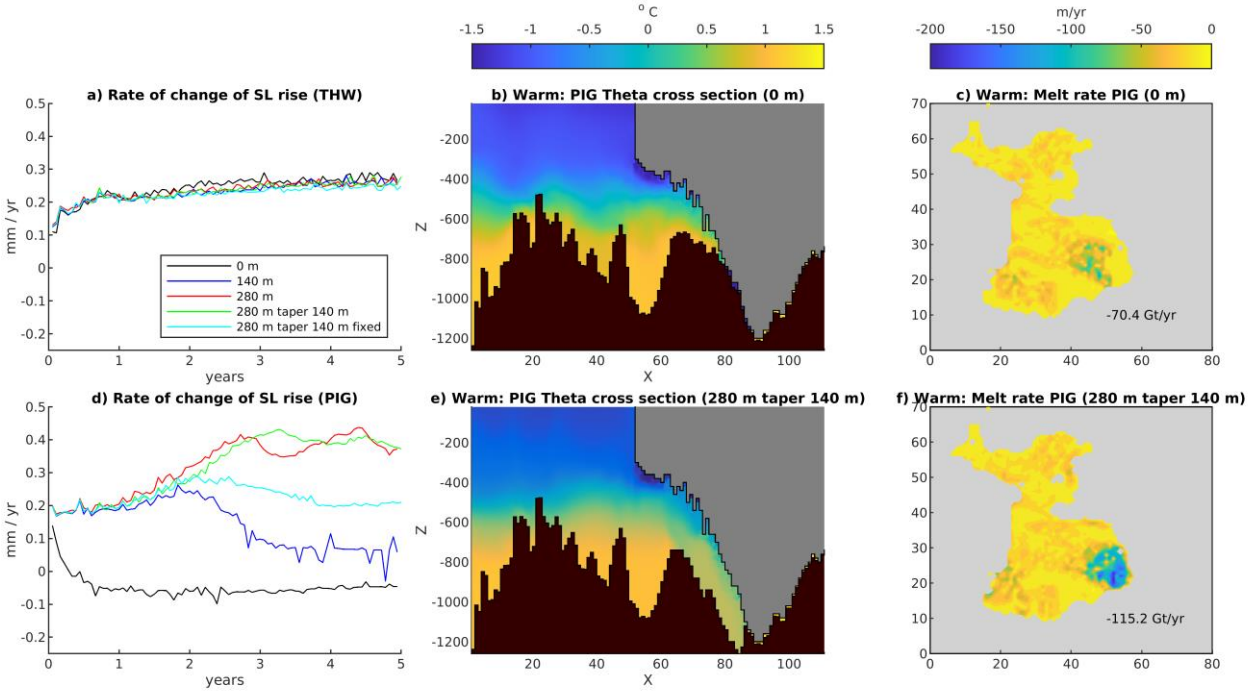

FIGURE B1: a) SLR rate of change for the Thwaites area for: zero digging, 140 m digging, 280 m digging, 280 m digging taper to 140 m over 6 km, and 280 m digging taper to 140 m fixed to initial melt rates. b) Cross-section through PIG Ice Shelf (taken along the green line shown in Figure 2a) showing initial potential temperature in the warm case in the zero-digging setup. c) Initial melt rate over PIG Ice Shelf in the warm forcing case for the zero-digging setup. d) Same as a) but for the PIG area. e) Same as (b), but for the 280 m taper 140 m digging setup. f) Same as (c), but for the 280m taper 140 m digging setup.

Appendix C: SLR compared against integrated melt

A strong correlation is found when comparing the sea level contribution against the integrated melt for both forcing cases in the areas of Thwaites and PIG (Figure C1). However, no variation to the oceanic boundary forcing is applied during the simulations and hence only geometric induced changes in the ice shelf melt rates can occur. These strong correlations are due to the melt rate and rate of change of SLR being approximately constant from PIG's area and having an approximately linear trend from Thwaites's area.

https://doi.org/10.5194/tc-2023-77
Preprint. Discussion started: 9 June 2023

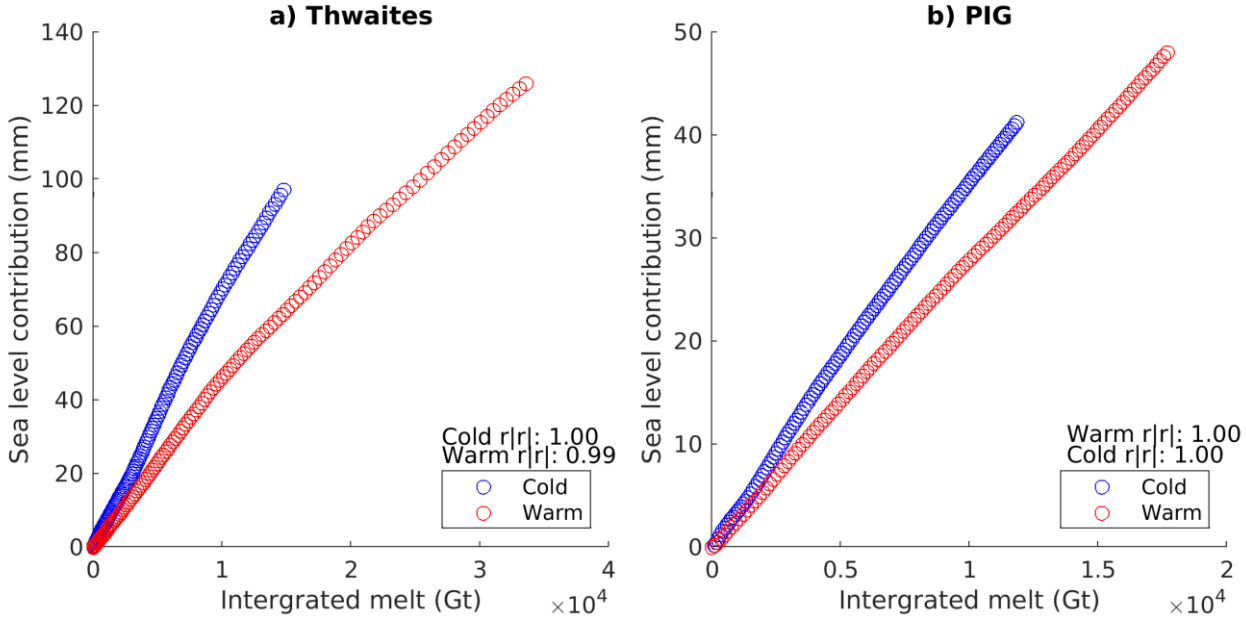

FIGURE C1: (a) Yearly points of sea level contribution plotted against integrated melt from the Thwaites area for the warm (red) and cold (blue) forced cases. (b) as in (a), but for the PIG area. In both, correlation coefficients are shown for the warm and cold cases.

Code and data availability

The version of MITgcm used in this study is available at https://github.com/David-Bett4/MITgcm/tree/Coupling_wHoriz_lat_Pchild_new_divout. The version of WAVI used in this study is available at https://github.com/RJArthern/WAVI.jl/tree/MITgcm_coupling. Coupling scripts and input text files are available at https://github.com/David-Bett4/MITgcm_WAVI_coupling. The model output underlying the figures and calculations in this paper is available at https://github.com/David-Bett4/Amundsen_coupling_paper.

Author contribution

DTB implemented coupling, set up ocean initial state, ran coupled simulations, performed analysis and led the manuscript. ATB and CRW set up initial WAVI ice model states and performed WAVI ice model relaxation simulations. RJA, PRH, and DNG designed and supervised the project. All of the co-authors contributed to coupling design, experiment design and edited the manuscript.

https://doi.org/10.5194/tc-2023-77
Preprint. Discussion started: 9 June 2023

Competing interests

The authors declare that they have no conflict of interest.

Acknowledgements

DTB, ATB, CRW, PRH, RJA were supported by the NERC Grant NE/S010475/1. CRW was partly funded by the MELT project, a component of the International Thwaites Glacier Collaboration (ITGC), with support from National Science Foundation (NSF: Grant no. 1739003) and Natural Environment Research Council (NERC: Grant no. NE/S006656/1). ITGC Contribution No. ITGC-108. This work used the ARCHER2 UK National Supercomputing Service (https://www.archer2.ac.uk).

References

Alevropoulos-Borrill, A. V., Nias, I. J., Payne, A. J., Golledge, N. R., and Bingham, R. J.: Ocean-forced evolution of the Amundsen Sea catchment, West Antarctica, by 2100, The Cryosphere, 14, 1245-1258, 10.5194/tc-14-1245-2020, 2020.

Arthern, R. J. and Williams, C. R.: The sensitivity of West Antarctica to the submarine melting feedback, Geophysical Research Letters, 44, 2352-2359, https://doi.org/10.1002/2017GL072514, 2017.

Arthern, R. J., Hindmarsh, R. C. A., and Williams, C. R.: Flow speed within the Antarctic ice sheet and its controls inferred from satellite observations, Journal of Geophysical Research: Earth Surface, 120, 1171-1188, https://doi.org/10.1002/2014JF003239, 2015.

Arthern, R. J., Winebrenner, D. P., and Vaughan, D. G.: Antarctic snow accumulation mapped using polarization of 4.3-cm wavelength microwave emission, Journal of Geophysical Research: Atmospheres, 111, https://doi.org/10.1029/2004JD005667, 2006.

Asay-Davis, X. S., Jourdain, N. C., and Nakayama, Y.: Developments in Simulating and Parameterizing Interactions Between the Southern Ocean and the Antarctic Ice Sheet, Current Climate Change Reports, 3, 316-329, 10.1007/s40641-017-0071-0, 2017.

Bett, D. T., Holland, P. R., Naveira Garabato, A. C., Jenkins, A., Dutrieux, P., Kimura, S., and Fleming, A.: The Impact of the Amundsen Sea Freshwater Balance on Ocean Melting of the West Antarctic Ice Sheet, Journal of Geophysical Research: Oceans, 125, e2020JC016305, https://doi.org/10.1029/2020JC016305, 2020.

Bradley, A. T., Bett, D. T., Dutrieux, P., De Rydt, J., and Holland, P. R.: The Influence of Pine Island Ice Shelf Calving on Basal Melting, Journal of Geophysical Research: Oceans, 127, e2022JC018621, https://doi.org/10.1029/2022JC018621, 2022.

Brondex, J., Gillet-Chaulet, F., and Gagliardini, O.: Sensitivity of centennial mass loss projections of the Amundsen basin to the friction law, The Cryosphere, 13, 177-195, 10.5194/tc-13-177-2019, 2019.

Cornford, S. L., Seroussi, H., Asay-Davis, X. S., Gudmundsson, G. H., Arthern, R., Borstad, C., Christmann, J., Dias dos Santos, T., Feldmann, J., Goldberg, D., Hoffman, M. J., Humbert, A., Kleiner, T., Leguy, G., Lipscomb, W. H., Merino, N., Durand, G., Morlighem, M., Pollard, D., Rückamp, M., Williams, C. R., and Yu, H.: Results of the third Marine Ice Sheet Model Intercomparison Project (MISMIP+), The Cryosphere, 14, 2283-2301, 10.5194/tc-14-2283-2020, 2020.

De Rydt, J., Holland, P. R., Dutrieux, P., and Jenkins, A.: Geometric and oceanographic controls on melting beneath Pine Island Glacier, Journal of Geophysical Research: Oceans, 119, 2420-2438, https://doi.org/10.1002/2013JC009513, 2014.

De Rydt, J. and Gudmundsson, G. H.: Coupled ice shelf-ocean modeling and complex grounding line retreat from a seabed ridge, Journal of Geophysical Research: Earth Surface, 121, 865-880, https://doi.org/10.1002/2015JF003791, 2016.

Donat-Magnin, M., Jourdain, N. C., Spence, P., Le Sommer, J., Gallée, H., and Durand, G.: Ice-Shelf Melt Response to Changing Winds and Glacier Dynamics in the Amundsen Sea Sector, Antarctica, Journal of Geophysical Research: Oceans, 122, 10206-10224, https://doi.org/10.1002/2017JC013059, 2017.

Dutrieux, P., De Rydt, J., Jenkins, A., Holland, P. R., Ha, H. K., Lee, S. H., Steig, E. J., Ding, Q., Abrahamsen, E. P., and Schröder, M.: Strong Sensitivity of Pine Island Ice-Shelf Melting to Climatic Variability, Science, 343, 174-178, 10.1126/science.1244341, 2014.

Favier, L., Durand, G., Cornford, S. L., Gudmundsson, G. H., Gagliardini, O., Gillet-Chaulet, F., Zwinger, T., Payne, A. J., and Le Brocq, A. M.: Retreat of Pine Island Glacier controlled by marine ice-sheet instability, Nature Climate Change, 4, 117-121, 10.1038/nclimate2094, 2014.

Feldmann, J. and Levermann, A.: Collapse of the West Antarctic Ice Sheet after local destabilization of the Amundsen Basin, Proceedings of the National Academy of Sciences, 112, 14191-14196, doi:10.1073/pnas.1512482112, 2015.

Goldberg, D. N. and Heimbach, P.: Parameter and state estimation with a time-dependent adjoint marine ice sheet model, The Cryosphere, 7, 1659-1678, 10.5194/tc-7-1659-2013, 2013.

Goldberg, D. N. and Holland, P. R.: The Relative Impacts of Initialization and Climate Forcing in Coupled Ice Sheet-Ocean Modeling: Application to Pope, Smith, and Kohler Glaciers, Journal of Geophysical Research: Earth Surface, 127, e2021JF006570, https://doi.org/10.1029/2021JF006570, 2022.

Goldberg, D. N., Snow, K., Holland, P., Jordan, J. R., Campin, J. M., Heimbach, P., Arthern, R., and Jenkins, A.: Representing grounding line migration in synchronous coupling between a marine ice sheet model and a z-coordinate ocean model, Ocean Modelling, 125, 45-60, https://doi.org/10.1016/j.ocemod.2018.03.005, 2018.

Graham, A. G. C., Wåhlin, A., Hogan, K. A., Nitsche, F. O., Heywood, K. J., Totten, R. L., Smith, J. A., Hillenbrand, C.-D., Simkins, L. M., Anderson, J. B., Wellner, J. S., and Larter, R. D.: Rapid retreat of Thwaites Glacier in the pre-satellite era, Nature Geoscience, 15, 706-713, 10.1038/s41561-022-01019-9, 2022.

Gudmundsson, G. H., Barnes, J. M., Goldberg, D. N., and Morlighem, M.: Limited Impact of Thwaites Ice Shelf on Future Ice Loss From Antarctica, Geophysical Research Letters, 50, e2023GL102880, https://doi.org/10.1029/2023GL102880, 2023.

Holland, D. M. and Jenkins, A.: Modeling Thermodynamic Ice–Ocean Interactions at the Base of an Ice Shelf, Journal of Physical Oceanography, 29, 1787-1800, https://doi.org/10.1175/1520-0485(1999)029<1787:MTIOIA>2.0.CO;2, 1999.

Holland, P. R. and Feltham, D. L.: The Effects of Rotation and Ice Shelf Topography on Frazil-Laden Ice Shelf Water Plumes, Journal of Physical Oceanography, 36, 2312-2327, https://doi.org/10.1175/JPO2970.1, 2006.

Holland, P. R., Bracegirdle, T. J., Dutrieux, P., Jenkins, A., and Steig, E. J.: West Antarctic ice loss influenced by internal climate variability and anthropogenic forcing, Nature Geoscience, 12, 718-724, 10.1038/s41561-019-0420-9, 2019.

Holland, P. R., O'Connor, G. K., Bracegirdle, T. J., Dutrieux, P., Naughten, K. A., Steig, E. J., Schneider, D. P., Jenkins, A., and Smith, J. A.: Anthropogenic and internal drivers of wind changes over the Amundsen Sea, West Antarctica, during the 20th and 21st centuries, The Cryosphere, 16, 5085-5105, 10.5194/tc-16-5085-2022, 2022.

Jacobs, S. S., Hellmer, H. H., and Jenkins, A.: Antarctic ice sheet melting in the Southeast Pacific, Geophysical Research Letters, 23, 957-960, Doi 10.1029/96gl00723, 1996.

Jenkins, A., Nicholls, K. W., and Corr, H. F. J.: Observation and Parameterization of Ablation at the Base of Ronne Ice Shelf, Antarctica, Journal of Physical Oceanography, 40, 2298-2312, https://doi.org/10.1175/2010JPO4317.1, 2010.

Jenkins, A., Shoosmith, D., Dutrieux, P., Jacobs, S., Kim, T. W., Lee, S. H., Ha, H. K., and Stammerjohn, S.: West Antarctic Ice Sheet retreat in the Amundsen Sea driven by decadal oceanic variability, Nature Geoscience, 11, 733-738, 10.1038/s41561-018-0207-4, 2018.

Jordan, J. R., Holland, P. R., Goldberg, D., Snow, K., Arthern, R., Campin, J.-M., Heimbach, P., and Jenkins, A.: Ocean-Forced Ice-Shelf Thinning in a Synchronously Coupled Ice-Ocean Model, Journal of Geophysical Research: Oceans, 123, 864-882, https://doi.org/10.1002/2017JC013251, 2018.

Joughin, I., Smith, B. E., and Medley, B.: Marine Ice Sheet Collapse Potentially Under Way for the Thwaites Glacier Basin, West Antarctica, Science, 344, 735-738, 10.1126/science.1249055, 2014.

Joughin, I., Shapero, D., Smith, B., Dutrieux, P., and Barham, M.: Ice-shelf retreat drives recent Pine Island Glacier speedup, Science Advances, 7, eabg3080, 10.1126/sciadv.abg3080, 2021.

Jourdain, N. C., Mathiot, P., Burgard, C., Caillet, J., and Kittel, C.: Ice Shelf Basal Melt Rates in the Amundsen Sea at the End of the 21st Century, Geophysical Research Letters, 49, e2022GL100629, https://doi.org/10.1029/2022GL100629, 2022.

Jourdain, N. C., Mathiot, P., Merino, N., Durand, G., Le Sommer, J., Spence, P., Dutrieux, P., and Madec, G.: Ocean circulation and sea-ice thinning induced by melting ice shelves in the Amundsen Sea, Journal of Geophysical Research: Oceans, 122, 2550-2573, https://doi.org/10.1002/2016JC012509, 2017.

Kimura, S., Jenkins, A., Regan, H., Holland, P. R., Assmann, K. M., Whitt, D. B., Van Wessem, M., van de Berg, W. J., Reijmer, C. H., and Dutrieux, P.: Oceanographic Controls on the Variability of Ice-Shelf Basal Melting and Circulation of Glacial Meltwater in the Amundsen Sea Embayment, Antarctica, Journal of Geophysical Research: Oceans, 122, 10131-10155, https://doi.org/10.1002/2017JC012926, 2017.

Lhermitte, S., Sun, S., Shuman, C., Wouters, B., Pattyn, F., Wuite, J., Berthier, E., and Nagler, T.: Damage accelerates ice shelf instability and mass loss in Amundsen Sea Embayment, Proceedings of the National Academy of Sciences, 117, 24735-24741, doi:10.1073/pnas.1912890117, 2020.

Marshall, J., Hill, C., Perelman, L., and Adcroft, A.: Hydrostatic, quasi-hydrostatic, and nonhydrostatic ocean modeling, Journal of Geophysical Research: Oceans, 102, 5733-5752, https://doi.org/10.1029/96JC02776, 1997.

Morlighem, M.: MEaSUREs BedMachine Antarctica, Version 3 [dataset], https://doi.org/10.5067/FPSU0V1MWUB6, 2022.

Morlighem, M., Rignot, E., Binder, T., Blankenship, D., Drews, R., Eagles, G., Eisen, O., Ferraccioli, F., Forsberg, R., Fretwell, P., Goel, V., Greenbaum, J. S., Gudmundsson, H., Guo, J., Helm, V., Hofstede, C., Howat, I., Humbert, A., Jokat, W., Karlsson, N. B., Lee, W. S., Matsuoka, K., Millan, R., Mouginot, J., Paden, J., Pattyn, F., Roberts, J., Rosier, S., Ruppel, A., Seroussi, H., Smith, E. C., Steinhage, D., Sun, B., Broeke, M. R. v. d., Ommen, T. D. v., Wessem, M. v., and Young, D. A.: Deep glacial troughs and stabilizing ridges unveiled beneath the margins of the Antarctic ice sheet, Nature Geoscience, 13, 132-137, 10.1038/s41561-019-0510-8, 2020.

Mouginot, J., Rignot, E., and Scheuchl, B.: Sustained increase in ice discharge from the Amundsen Sea Embayment, West Antarctica, from 1973 to 2013, Geophysical Research Letters, 41, 1576-1584, https://doi.org/10.1002/2013GL059069, 2014.

https://doi.org/10.5194/tc-2023-77
Preprint. Discussion started: 9 June 2023

Mouginot, J., Scheuchl, B., and Rignot, E.: MEaSUREs Annual Antarctic Ice Velocity Maps, Version 1 [dataset], https://doi.org/10.5067/9T4EPQXTJYW9, 2017a.
Mouginot, J., Rignot, E., Scheuchl, B., and Millan, R.: Comprehensive Annual Ice Sheet Velocity Mapping Using Landsat-8, Sentinel-1, and RADARSAT-2 Data, 10.3390/rs9040364, 2017b.
Naughten, K. A., De Rydt, J., Rosier, S. H. R., Jenkins, A., Holland, P. R., and Ridley, J. K.: Two-timescale response of a large Antarctic ice shelf to climate change, Nature Communications, 12, 1991, 10.1038/s41467-021-22259-0, 2021.
Naughten, K. A., Holland, P. R., Dutrieux, P., Kimura, S., Bett, D. T., and Jenkins, A.: Simulated Twentieth-Century Ocean Warming in the Amundsen Sea, West Antarctica, Geophysical Research Letters, 49, e2021GL094566, https://doi.org/10.1029/2021GL094566, 2022.
Nias, I. J., Cornford, S. L., Edwards, T. L., Gourmelen, N., and Payne, A. J.: Assessing Uncertainty in the Dynamical Ice Response to Ocean Warming in the Amundsen Sea Embayment, West Antarctica, Geophysical Research Letters, 46, 11253-11260, https://doi.org/10.1029/2019GL084941, 2019.
Otosaka, I. N., Shepherd, A., Ivins, E. R., Schlegel, N. J., Amory, C., van den Broeke, M. R., Horwath, M., Joughin, I., King, M. D., Krinner, G., Nowicki, S., Payne, A. J., Rignot, E., Scambos, T., Simon, K. M., Smith, B. E., Sørensen, L. S., Velicogna, I., Whitehouse, P. L., A, G., Agosta, C., Ahlstrøm, A. P., Blazquez, A., Colgan, W., Engdahl, M. E., Fettweis, X., Forsberg, R., Gallée, H., Gardner, A., Gilbert, L., Gourmelen, N., Groh, A., Gunter, B. C., Harig, C., Helm, V., Khan, S. A., Kittel, C., Konrad, H., Langen, P. L., Lecavalier, B. S., Liang, C. C., Loomis, B. D., McMillan, M., Melini, D., Mernild, S. H., Mottram, R., Mouginot, J., Nilsson, J., Noël, B., Pattle, M. E., Peltier, W. R., Pie, N., Roca, M., Sasgen, I., Save, H. V., Seo, K. W., Scheuchl, B., Schrama, E. J. O., Schröder, L., Simonsen, S. B., Slater, T., Spada, G., Sutterley, T. C., Vishwakarma, B. D., van Wessem, J. M., Wiese, D., van der Wal, W., and Wouters, B.: Mass balance of the Greenland and Antarctic ice sheets from 1992 to 2020, Earth Syst. Sci. Data, 15, 1597-1616, 10.5194/essd-15-1597-2023, 2023.
Pattyn, F.: Antarctic subglacial conditions inferred from a hybrid ice sheet/ice stream model, Earth and Planetary Science Letters, 295, 451-461, https://doi.org/10.1016/j.epsl.2010.04.025, 2010.
Reese, R., Levermann, A., Albrecht, T., Seroussi, H., and Winkelmann, R.: The role of history and strength of the oceanic forcing in sea level projections from Antarctica with the Parallel Ice Sheet Model, The Cryosphere, 14, 3097-3110, 10.5194/tc-14-3097-2020, 2020.
Seroussi, H. and Morlighem, M.: Representation of basal melting at the grounding line in ice flow models, The Cryosphere, 12, 3085-3096, 10.5194/tc-12-3085-2018, 2018.
Seroussi, H., Nakayama, Y., Larour, E., Menemenlis, D., Morlighem, M., Rignot, E., and Khazendar, A.: Continued retreat of Thwaites Glacier, West Antarctica, controlled by bed topography and ocean circulation, Geophysical Research Letters, 44, 6191-6199, https://doi.org/10.1002/2017GL072910, 2017.
Shepherd, A., Gilbert, L., Muir, A. S., Konrad, H., McMillan, M., Slater, T., Briggs, K. H., Sundal, A. V., Hogg, A. E., and Engdahl, M. E.: Trends in Antarctic Ice Sheet Elevation and Mass, Geophysical Research Letters, 46, 8174-8183, https://doi.org/10.1029/2019GL082182, 2019.
Smith, B., Fricker, H. A., Gardner, A. S., Medley, B., Nilsson, J., Paolo, F. S., Holschuh, N., Adusumilli, S., Brunt, K., Csatho, B., Harbeck, K., Markus, T., Neumann, T., Siegfried, M. R., and Zwally, H. J.: Pervasive ice sheet mass loss reflects competing ocean and atmosphere processes, Science, 368, 1239-1242, 10.1126/science.aaz5845, 2020.
Thomas, R. H.: The Dynamics of Marine Ice Sheets, Journal of Glaciology, 24, 167-177, 10.3189/S0022143000014726, 1979.
Walker, D. P., Brandon, M. A., Jenkins, A., Allen, J. T., Dowdeswell, J. A., and Evans, J.: Oceanic heat transport onto the Amundsen Sea shelf through a submarine glacial trough, Geophysical Research Letters, 34, Artn L02602 10.1029/2006gl028154, 2007.
Weertman, J.: The Theory of Glacier Sliding, Journal of Glaciology, 5, 287-303, 10.3189/S0022143000029038, 1964.
Wild, C. T., Alley, K. E., Muto, A., Truffer, M., Scambos, T. A., and Pettit, E. C.: Weakening of the pinning point buttressing Thwaites Glacier, West Antarctica, The Cryosphere, 16, 397-417, 10.5194/tc-16-397-2022, 2022.
Yu, H., Rignot, E., Seroussi, H., and Morlighem, M.: Retreat of Thwaites Glacier, West Antarctica, over the next 100 years using various ice flow models, ice shelf melt scenarios and basal friction laws, The Cryosphere, 12, 3861-3876, 10.5194/tc-12-3861-2018, 2018.